Journal of Alloys and Compounds 509 (2011) 4653–4659

Contents lists available at ScienceDirect

Journal of Alloys and Compounds

journal homepage: www.elsevier.com/locate/jallcom

DySb under high pressures: A full-potential study

Dinesh C. Gupta*, Subhra Kulshrestha

Condensed Matter Theory Group, School of Studies in Physics, Jiwaji University, Gwalior, 474 011 M.P., India

ARTICLE INFO

Article history:
Received 27 July 2010
Received in revised form 5 January 2011
Accepted 30 January 2011
Available online 22 February 2011

Keywords:
Rare-earth compounds
Phase transition
Electronic properties
Elastic properties
Magnetic properties
High pressure

ABSTRACT

The magnetic, structural, electronic and mechanical properties of DySb in the stable $Fm\bar{3}m$ and high-pressure $Fm\bar{3}m$ phase have been analyzed using full potential (linear) augmented plane wave method. The local spin-density approximation along with Hubbard-U corrections and spin–orbit coupling has been used for present calculations. The magnetic phase stability shows that DySb is ferromagnetically stable at ambient and high pressures. Under compression, it undergoes first-order structural transition from B1 to B2 phase at 22.2 GPa which shows good agreement with the experimental value of ~22 GPa. The elastic properties of DySb have also been computed at normal and high pressures. The structural properties *viz*, equilibrium lattice constant, bulk modulus and its pressure derivative, transition pressure, volume collapse and elastic moduli are in good agreement with the experimental data. The calculation shows DySb to be semi-metallic.

1. Introduction

In recent years, the rare-earth (RE) compounds with rock-salt structure have drawn considerable interests of materials scientists due to their diverse structural, transport, magnetic and vibrational properties [1–16]. Spurred by the search for magnetic semiconductors *i.e.*, spintronic materials, we now have a better understanding of the electronic, magnetic and transport properties of RE compounds which are, generally, semiconductors or semimetals. Despite their simple rock-salt structure, they demonstrate various types of magnetic ordering. Their electronic structures and magnetic properties are sensitive to temperature, pressure (strain) and impurity effects. The RE 4*f*–5*d* interactions and the hybridizations between the RE non-4*f* and pnictogen *p* states are responsible for many fascinating phenomena that occur in them. In contrast to the RE metals, both super exchange and indirect Ruderman–Kittel–Kasuya–Yosida (RKKY) type interactions coexist in the family of RE compounds while the former interaction is dominant in heavy RE monopnictides. It is possible that other exchange coupling mechanisms, such as direct exchange or double exchange or both may also contribute in these monopnictides.

DySb constitutes an interesting system due to strongly correlated electrons with partially filled *f* orbitals of Dy atom which is found to be responsible for its anomalous properties. The changing 4*f* occupation implies that the RE elements and hence their compounds show different magnetic properties and electronic structures. Due to the unfilled 4*f* shells of Dy atom, it is a challenging problem to obtain an accurate theoretical description of the electronic structure of DySb.

The total magnetic moments have both orbital and spin components because *f* orbital moments cannot be quenched by the crystal field, hence spin–orbital interactions are particularly strong for many of the RE elements and compounds. The inner shell magnetic moments are largely aligned through intra-atomic *s*(*d*)–*f* exchange interaction and weaker inter-atomic *s*–*s* (*d*–*d*) exchange interactions. The 4*f* bands are generally very narrow and significantly different from the bands dominated by *s*, *p* and *d* states; there exists strong on-site Coulomb repulsion between the highly localized *f* electrons [17 and references therein]. This makes the independent particle approximation no longer valid and calculations based on local spin density approximation (LSDA) fail to describe the RE 4*f* electrons correctly. To explain the behavior of RE 4*f* electrons, many-body effects must be taken into account and calculations beyond LSDA are absolutely necessary. Coulomb repulsion (U) as an additional parameter to the one particle LSDA equations for a quasi-particle band structure can be introduced for this purpose.

The high pressure structural behavior of binary RE compounds is of current interest in condensed matter research. The majority of these compounds undergo first-order structural transition from NaCl (B1 phase) to CsCl (B2 phase) structure at high pressures. Recently, Shirotani et al. [1] have investigated the high pressure structural properties in these compounds up to 60 GPa at room temperature by powder X-ray diffraction (XRD) using synchrotron radiation whose profile shows that DySb is stable in NaCl structure at ambient conditions and transform to CsCl structure at ~22 GPa.

* Corresponding author. Tel.: +91 751 2442777; fax: +91 751 2442787.
E-mail addresses: sosfizix@gmail.com, sosfizix@yahoo.co.in (D.C. Gupta).

0925-8388/$ – see front matter © 2011 Elsevier B.V. All rights reserved.
doi:10.1016/j.jallcom.2011.01.175

The aim of the present computation is to perform a comprehensive study of the structural, magnetic, mechanical and electronic properties of DySb. A survey of the literature reveals that no theoretical attempts have been devoted so far to predict these properties of DySb. For making a better account of the on-site *f*-electron correlations, we have adopted a suitable LSDA + U approach [18].

The present article has been organized as: A brief description of the methodology used to compute parameters has been given in the next section followed by discussion on the calculated results, on a variety of interesting physical properties, in Section 3. The paper is concluded in Section 4.

2. Theory and method of calculation

A variety of material properties of DySb have been computed by employing first principles full-potential (linear) augmented plane wave + local orbital (FP-L/APW + lo) method [19] using the WIEN2K code [20] within the frame work of density functional theory [21]. In this method, the unit cell is divided into non-overlapping spheres centered at atomic sites (muffin-tin (MT) spheres) of radius (R_{MT}) and an interstitial region. In the MT spheres, the Kohn–Sham wave functions are expanded as a linear combination of radial functions × spherical harmonics, and in the remaining space of the unit cell a plane wave basis set is chosen. The basis set inside each MT sphere split into core and valence subsets. The core states are treated within the spherical part of the potential only and are assumed to have spherically symmetric charge density totally confined inside the MT spheres. The valence part is treated within a potential expanded into spherical harmonics. The Dy ($6s^2\ 5p^6\ 5d^1\ 4f^9$) and Sb ($4d^{10}\ 5s^2\ 5p^3$) states are treated as valence electrons. We have used 9 as the value for the parameter $R_{MT}K_{max}$ which determines the matrix size, where K_{max} is the plane wave cut-off and R_{MT} is the MT radius. The valence wave functions inside MT spheres were expanded up to $l_{max} = 10$, while the charge density was Fourier expanded up to $G_{max} = 14\ (a.u.)^{-1}$. All calculations were spin polarized. For the exchange correlation potential, the LDA form was adopted [22]. To improve the description of Dy 4*f* electrons, we used the LSDA + U (on-site coulomb interaction) method [18]. In the LSDA + U-like methods, an orbital dependent potential is introduced for the chosen set of electron states, which in our case are 4*f* states of Dy. This additional potential has an atomic Hartree–Fock form but with screened Coulomb and exchange interaction parameters. The coulomb potential $U = 6.3$ eV and the exchange coupling $J = 0.1$ eV for the Dy 4*f* orbitals has been calculated in the super cell approximation using the method proposed by Madsen and Novak [23]. The fully localized limit version of the LSDA + U method has been employed. The spin–orbit coupling (SOC) was included on the basis of the second variational method by using a scalar relativistic wave functions [20]. A mesh of 4096 special k-points was taken in the irreducible wedge of the Brillouin zone. The iteration process was repeated until the calculated total energy of the material converged to less than 0.5 mRy/unit cell.

3. Results and discussion

3.1. Magnetic stability

To test the magnetic stability of the material at ambient conditions, we have performed the self-consistent calculations of total energy for non-magnetic (NM) and magnetic (M) states of DySb in B1 phase. For this purpose, the minimisation technique has been used to obtain the optimised values of the total energy at ambient and high pressure conditions. The optimised values of total energy thus computed in both NM and M states were fitted to the Murnaghan's equation of state [24] $V/V_0 = (1 + (B_0'/B_0)P)^{-1/B_0'}$ to obtain the pressure–volume relationship with B_0 ($=-V(\partial P/\partial V)_T$) as the equilibrium bulk modulus ($=(\partial B_0/\partial P)_T$) as its first-order pressure derivative and P ($=-\partial E/\partial V$) as the pressure which is defined as the negative derivative of the total energy. From the calculations, it is clear that the energies in NM and M states do not intersect each other and the total energy remains lower in M phase, hence ferromagnetic (FM) state is stable at ambient as well as at high pressures. The equilibrium cell volume in the FM state at ambient pressure has been estimated as 386.66 a.u.^{3} which is very close to the experimental data (390.46 a.u.^{3}) [1].

Table 1
The values of lattice parameter (a in Å), bulk modulus (B_0 in GPa) and its pressure derivative (B_0') of DySb in B1 and B2 phases.

a	B_0	B_0'	References
B1 phase			
6.12	61.68	4.12	Present
6.14, 6.16	–	–	Expt. [1,2]
~6.16	64.49[a]	–	Others [7]
B2 phase			
3.69	66.51	3.74	Present

[a] Ref. [9].

3.2. Phase transition properties

To compute the phase transition properties of DySb, the total energy of the system has been computed self-consistently as a function of volume for B1 and B2 phases in FM state. The calculated results in B1 and B2 phases are plotted in Fig. 1. It is seen from this figure that it is stable in B1 phase at ambient conditions due to the fact that the energy in this phase is lower as compared to that in B2 phase. On further compression, beyond B1 → B2 transformation, the energy of B2 phase depresses more as compared to that of B1 phase showing first-order phase transition at high pressures which is consistent with experiments [1]. It is clear from this figure that convergence occurs at a value very close to the experimental lattice constant. The correct description of lattice constant confirms that the interactions considered in the present computation and the process of self-consistent field approach are capable of predicting correctly the minimum total energy of the compound in the parent (B1) phase. The calculated values of equilibrium lattice parameter, bulk modulus and its pressure derivative have been presented in Table 1 and compared with available experimental [1] and other theoretical [7] data.

The calculated value of equilibrium lattice constant deviates marginally by 0.3% from the measured value for DySb. This variation lies within the limits of DFT with LSDA. Under ambient conditions, it crystallizes in B1 phase with bulk modulus ($B_0 = 61.68$ GPa) which is smaller than the value ($B_0 = 66.51$ GPa) in the compressed B2 phase. The values of B_0 and its pressure derivative (B_0') are of academic interest at present due to non-availability of measured data.

To determine the phase transition pressure at $T = 0$ K (*i.e.*, ignoring the entropy of the crystal), Gibbs free (GF) energies ($G = E + PV$) of B1 and B2 phases have been calculated at different pressures. The pressure at which the two GF energies cross each other *i.e.*, ΔG ($=G_{B2} - G_{B1}$) becomes zero has been indicated as phase transition pressure (P_T). It is clear from Fig. 1 that at zero pressure, the B1 phase is a thermodynamically stable state and remains stable until the pressure reaches P_T (=22.2 GPa). At pressures above P_T, the B2 phase becomes stable with more minimum GF energy while the B1 phase becomes thermodynamically unstable with comparatively higher GF energy.

We have plotted the variation of reduced volume ($V(P)/V(0)$) with pressure (P) to get the equation of state/phase diagram in Fig. 2 for DySb along with the available experimental data. It is clear from this figure that the volume decreases smoothly up to

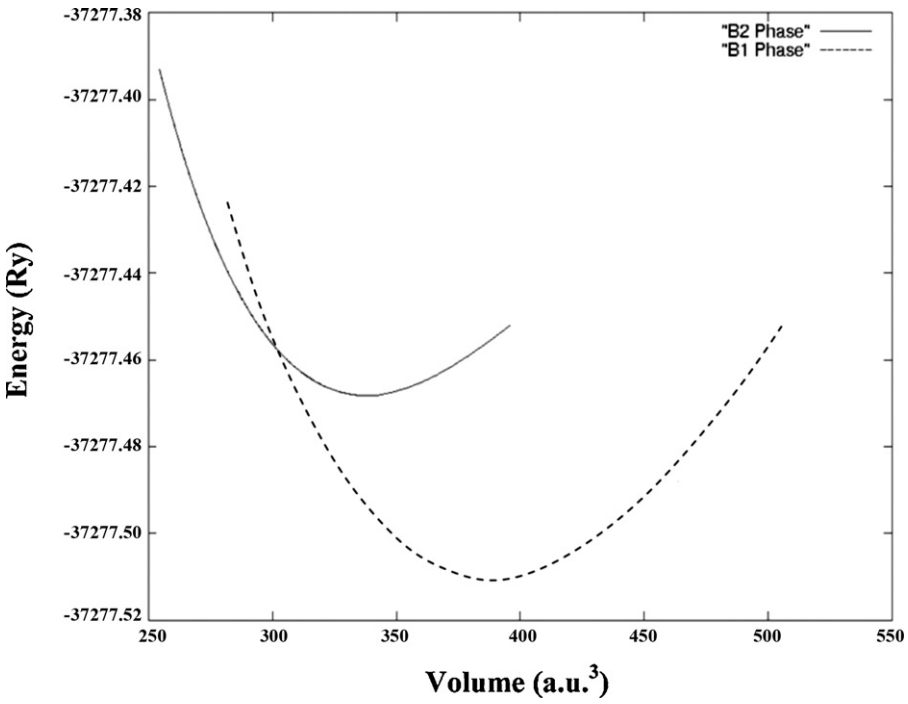

Fig. 1. Total energy *vs.* cell volume in B1 and B2 phases of DySb calculated by LSDA + U.

22.2 GPa. At this pressure, an abrupt decline in volume is observed while similar change has been observed experimentally at ~22 GPa. This discontinuity is associated with first-order structural phase transformation (B1 → B2). The value of % volume collapse at P_T ($\Delta V(P_T)/V(0)$) is reported in Table 2 along with experimental data. It is seen that these values are quite close to the measured values [1].

3.3. Elastic properties

The elastic moduli have been calculated from the variation of the total energy under volume-conserving strains, on the lines as implemented in WIEN2K code [20].

The computed values of elastic moduli for DySb in B1 phase have been presented in Table 3 which satisfies all the necessary conditions for mechanical stability $(C_{11} - C_{12}) > 0$, $(C_{11} + 2C_{12}) > 0$, $C_{11} > 0$, $C_{44} > 0$ [25] for cubic crystal structures such as rock-salt; hence it is mechanically stable in B1 phase. Besides this, we have also computed various combinations of these second-order elastic constants *viz.*, shear and stiffness constant (C_S and C_L), isotropic shear (G), Young's (Y) moduli, Kleinman parameter (ξ), Poisson's ratio (σ), elastic anisotropy factor (A) and Cauchy's relation at ambient conditions by using the relations and conditions listed elsewhere [8]. Our values agree well with the measured data [2] and better than those calculated earlier by empirical model [9].

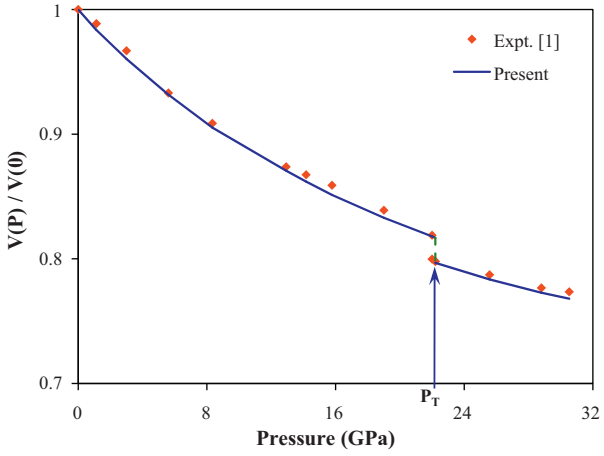

Fig. 2. Equation of state/phase diagram of DySb.

Table 2
The calculated values of the phase transition pressure (P_T in GPa), the % volume collapse at P_T ($\Delta V(P_T)/V(0)$), energy of structures at zero pressure with respect to the rock-salt phase (ΔG in Ry/unit cell/atom) and the equilibrium volume (V_0 in Å^3) for DySb.

Properties	Present	Expt. [1]	Others [9]
P_T	22.2	~22	23.6
$\Delta V(P_T)/V(0)$	2.00	1.91	6.8
	B1 phase		B2 phase
	Present	Expt. [1]	Present
ΔG	0.00	–	0.05
V_0	57.30	57.87	50.15

The ductile/brittle nature of the material may be distinguished on the basis of σ [26]; if it is ≤0.33 the material is brittle else ductile. Our calculated value of σ is below the critical value showing DySb to be brittle. The value of A lies well below unity and hence DySb is anisotropic. For metallic bonding, the Cauchy pressure must be positive while for directional bonding with angular character, it

Table 3
Calculated values of elastic properties (in GPa), and σ, A and ξ are dimensionless for DySb in B1 phase.

Parameters	Present	Expt. [2]	Others [9]
$C_{11}-C_{12}$	145.1	148.0	115.9
C_{44}	24.9	26.0	26.2
G	44.0	45.2	–
A	0.3	0.3	–
C_S	72.5	74.0	–

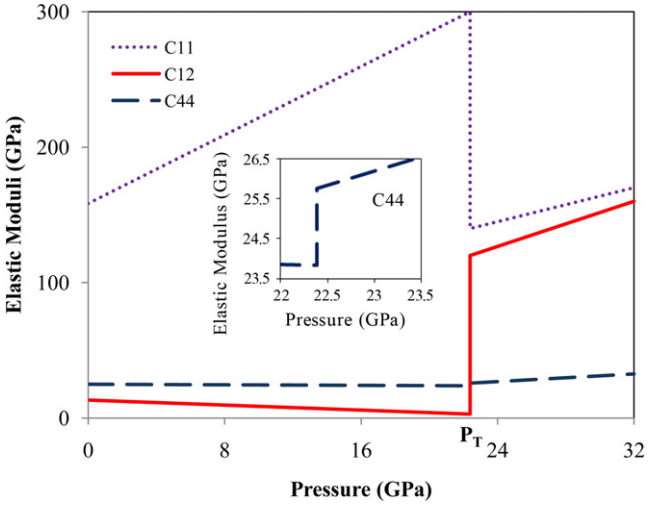

Fig. 3. Variation of elastic moduli with pressure for DySb.

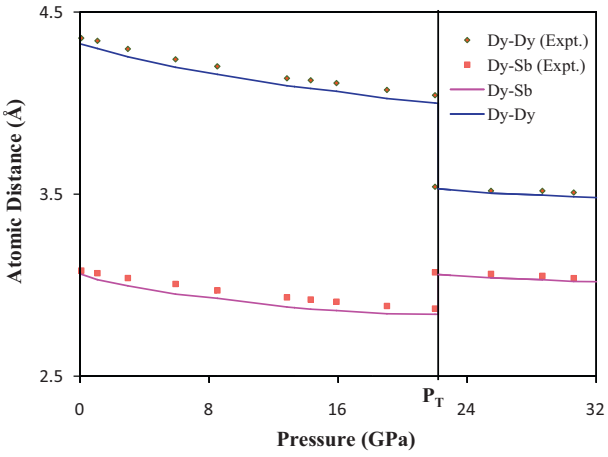

Fig. 4. Variation of atomic distances *vs.* pressure for DySb.

should be negative [27]. The calculated value of Cauchy pressure is −11.62 GPa which confirms directional nature (partial covalent) of DySb.

The pressure variation of the SOECs and their combinations in B1 and B2 phases has been shown in Fig. 3 to analyze the mechanical strength of DySb. It may be seen from this figure that C_{11} increases linearly in the B1 phase with an abrupt decline at P_T whereafter it again increases in B2 phase. The shear moduli (C_{12} and C_{44}) decrease with pressure followed by an abrupt increase at P_T although the variation in C_{44} is almost imperceptible as compared to other moduli. This decrease shows that the phase transition is accompanied by shear deformation arising due to lattice instability. It reflects the strong weakening of bonding forces. The pressure variation of σ (not reported here) shows decrease in B1 phase up to P_T followed by an abrupt jump at P_T beyond which it increases in B2 phase which shows that the material britility increases in B1 phase while the ductility starts dominating over it at P_T and further increases in B2 phase. Hence, the material which was brittle initially in parent phase (B1) becomes ductile in B2 phase.

To visualize the effect of pressure on the cation–cation and cation–anion distances, we have plotted the variation of Dy–Dy and Dy–Sb distance with pressure in Fig. 4. The Dy–Sb distance in B1 phase is 3.06 Å at the ambient pressure. This distance is much shorter than the sum of ionic radii of Dy^{3+} (0.99 Å) and Sb^{3-} (2.45 Å). The Dy–Sb distance is slightly shorter than the sum of the atomic radius of Dy (1.77 Å) and the covalent radius of Sb (1.38 Å), longer than the sum of the covalent radii of Dy (1.59 Å) and Sb (1.38 Å). Thus, the chemical bond between Dy and Sb atoms has the covalent character. When the B1–B2 transition occurs at 22.2 GPa, the Dy–Sb distance suddenly increases and becomes 3.058 Å in B2 phase. This agrees with the Dy–Sb distance (3.06 Å) in the NaCl-type structure at ambient pressure. It is clear that the Dy–Dy distance shows an abrupt decline at B1–B2 transition. This distance (3.53 Å) in B2 phase agrees with the sum of atomic radius of Dy (1.77 Å). On the other hand, Dy–Sb distance shows an abrupt increase at P_T. This increase in interionic distance gives rise to weakening of Coulomb force in B2 phase, also counteracted by nearest neighbour repulsive forces. The short-range repulsion due to next-nearest neighbours also decreases with pressure showing that the ions come closer with compression thereby giving rise to increase in the repulsion. This increase in repulsion due to the cation–cation is capable to deform the lattice by reconfiguring the atoms within the lattice, *i.e.*, structural change at transition pressure. It may be concluded that the cation in these compounds is more compressible as compared to anion at P_T and hence the Dy–Dy distance shows larger change as compared to Dy–Sb at P_T.

We have calculated the Debye temperature (θ_D) for DySb using [28,29] $\theta_D = (h/k_B)[3n/4\pi V_a]^{1/3}\upsilon_m$ where the constants have their

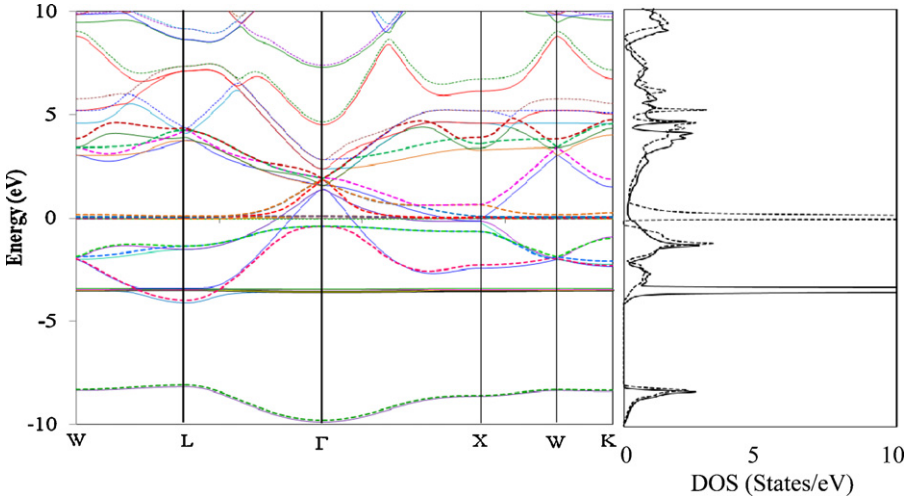

Fig. 5. Band structure and DOS of DySb for LSDA in B1 phase at ambient conditions. Solid lines; majority spin, dashed lines; minority spin. The position of the Fermi level is set at zero.

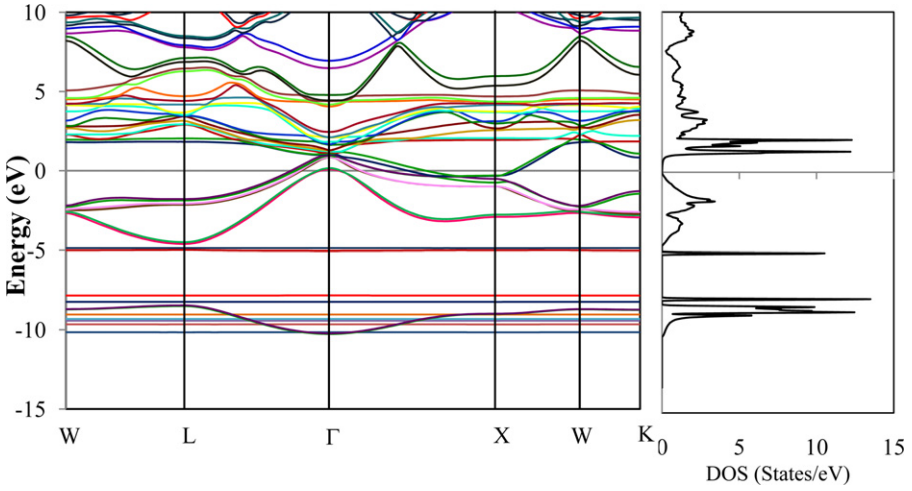

Fig. 6. Band structure and DOS of DySb for LSDA + U in B1 phase at ambient conditions. The position of the Fermi level is set at zero.

usual meanings. Here, V_a is atomic volume while average speed of sound (υ_m) in the polycrystalline material is given as $\upsilon_m = [(1/3)((2/\upsilon_t^3) + (1/\upsilon_l^3))]^{-1/3}$ with υ_l and υ_t as the longitudinal and transverse sound velocities, obtained by using SOECs (C_{11}, C_{12} and C_{44}) and ρ is the mass density per unit volume.

$$\upsilon_l = \sqrt{\frac{[C_{11} + (2/5)(2C_{44} + C_{12} - C_{11})]}{\rho}},$$

$$\upsilon_t = \sqrt{\frac{[C_{44} + (1/5)(2C_{44} + C_{12} - C_{11})]}{\rho}}$$

The calculated sound velocity and Debye temperature as well as the density for DySb are given in Table 4. The calculated values of θ_D are slightly higher than the experimental [2] values due to the fact that our value of density is larger than the experimental [2] value. Besides this, the discrepancy may be due to the fact that we have calculated these values at ambient conditions while the experimental data on elastic constants is available at 200 K on which Debye temperature [2] is based.

3.4. Electronic properties

The spin-polarized electronic structures have been investigated in B1 (at the equilibrium lattice constant) and B2 (just after the phase transition) using LSDA and LSDA + U schemes. The spin direction (↑ and ↓) is taken as the direction of the RE spins (majority ↑ and minority ↓). The full band structure and total density of states (DOS) within LSDA for DySb has been shown in Fig. 5 for majority (solid lines) and minority spins (dashed lines). The band structure of DySb in the FM state with on-site 4*f* Coulomb repulsion (Hubbard U) has also been calculated and shown in Fig. 6.

It is found that the LSDA + U strategy has significant impact on the overall LSDA band structure particularly on the energy levels of the occupied and unoccupied 4*f* states. In LSDA scheme, the occupied 4*f* states (spin up channel) are placed about 3.4–4 eV below E_F (Fig. 5) which are strongly hybridized with Sb 5*p* states, while the partially occupied 4*f* states (spin down channel) are located around 1 eV above E_F (Fig. 5). There is no direct photoemission data available for DySb single crystal but experiments have been performed on GdX (X = P, As, Sb, Bi) [30]. We have compared our

Table 4
The calculated values of density (ρ in gm/cm^3), the longitudinal, transverse and average sound velocity (υ_l, υ_t and υ_m in m/s) and Debye temperature (θ_D in K) for DySb in B1 phase.

Properties	Present	Expt. [2]
ρ	8.2	8.1
υ_l	3822.3	–
υ_t	2310.9	–
υ_m	2554.5	–
θ_D	249	241

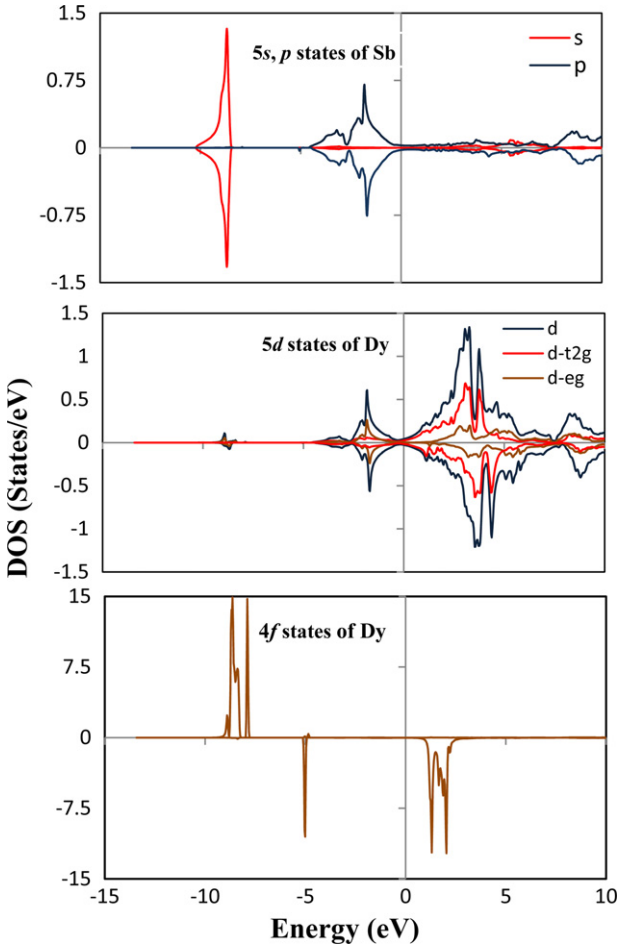

Fig. 7. The *l*-projected DOS of DySb for LSDA + U in B1 phase. Spin minority states are of negative values. The position of the Fermi level is set at zero.

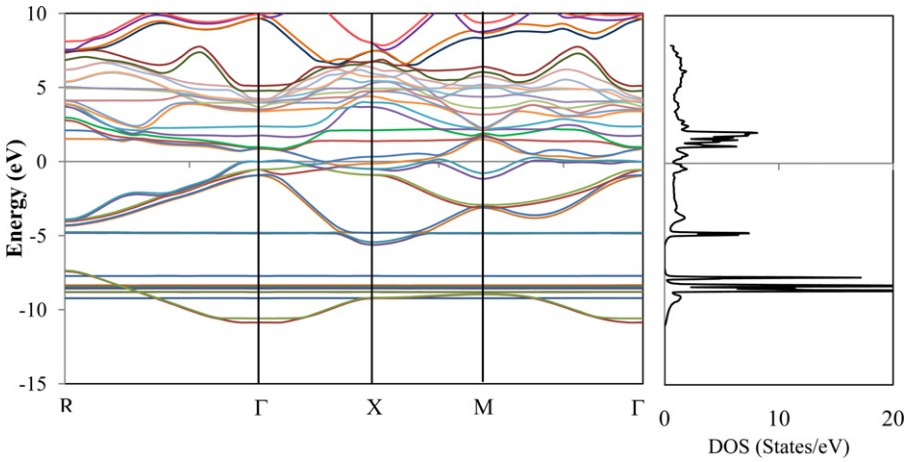

Fig. 8. Band structure and DOS of DySb for LSDA + U in B2 phase just after the phase transition. The position of the Fermi level is set at zero.

Table 5
Total and local magnetic moments (M and m) (Bohr magneton μ_B) as function of pressure (GPa) for DySb B1 and B2 phase.

Pressure	B1 phase				B2 phase			
	m^{Dy}	m^{Sb}	$m^{Interstitial}$	M	m^{Dy}	m^{Sb}	$m^{Interstitial}$	M
0	5.022	−0.022	0.307	5.307	5.023	−0.023	0.314	5.314
10	5.002	−0.027	0.323	5.298	5.003	−0.029	0.331	5.305
20	4.932	−0.031	0.384	5.285	4.936	−0.032	0.395	5.299
30	4.902	−0.035	0.415	5.282	4.904	−0.037	0.419	5.286

results with GdX because Dy is the second next element to Gd in the lanthanide series. Yamada et al. [30] have reported that in GdX the occupied and unoccupied 4*f* levels are situated around 8–10 eV below and 5–6 eV above E_F. Furthermore, the X-ray photoelectron spectroscopy (XPS) experiment on GdN shows that the Gd 4*f* levels lay 7.8 eV below E_F [31]. Thus the LSDA calculation fails to give the correct binding energies of the 4*f* energy levels. This situation is much improved by the LSDA + U method.

The band structure within the LSDA + $U_{f\text{-Dy}}$ scheme in B1 phase is shown in Fig. 6. It is observed that the crystal field splitting of Dy-4*f* bands within LSDA is quite small and difficult to identify due to hybridization with itinerant bands. From LSDA + U, all 4*f* majority states and two of the seven 4*f* minority states are occupied and reside 7.8–10.15 eV and around 5 eV below E_F and unoccupied 4*f* minority states are around 2 eV above E_F which are strongly hybridized with Dy 5*d* states.

The *l*-projected density of states (DOS) plot (Fig. 7) provides an even clearer picture of the elemental contributions to the electronic structure of DySb. In view of this figure, the bands lie around −8.7 eV are mainly due to Sb-5*s* states hybridized with occupied 4*f* majority states and those top valence states right below the Fermi level are predominantly Sb-5*p* states. The Dy 5*d* states, however, also make a noticeable contribution. In our calculation both 5*d* e_g and 5*d* t_{2g} states participate in the hybridization with Sb 5*p* states, though the contributions to the bottom of the conduction band(s) are dominated by 5*d* t_{2g} states. Here, we would like to catch the attention that the Dy 5*d*–Sb 5*p* hybridization is important in establishing the physical properties of DySb. This hybridization results in magnetic moments on pnictogen sites and is responsible for the intriguing magnetic orderings and transport properties. Another by-product of the above Dy 5*d*–Sb 5*p* hybridization is the induced magnetic moments on antimonide atoms. Actually, the induced magnetic moment on the pnictogen atom is a typical feature of RE monopnictides. It may also be seen from Fig. 6 that there is no gap appears between the Dy 5*d* and Sb 5*p* states at the Γ point for both the majority and minority spin hence we may say that DySb is seen to be semi-metallic.

To see the effect of high pressure on the electronic structure we have also computed the band structure and DOS in B2 phase (just after the B1 → B2 transition) and plotted in Fig. 8. It is seen that 5*p* states of Sb split under pressure, out of which some of them crosses E_F showing metallization. Furthermore, in spin-up channel, the *f* bands of Dy lie below the Fermi level similar to Fig. 6 except that they all come closer with decrease in *f* bandwidth. In spin-down channel, occupied *f*-bands lie below E_F and hybridized with 5*p* states of Sb while band broadening occurs in unoccupied *f*-bands (above E_F).

The spin-polarized self-consistent band structure calculations have been very successful in predicting the magnetic moments by LSDA + U scheme. The calculated values of magnetic moments in B1 and B2 phases are listed in Table 5. It is clear that the total and local magnetic moments (M and m) decrease with the increase in pressure except for the magnetic moment in the interstitial region. The contribution to the total magnetic moment is mainly due to 4*f* electrons of Dy, while the contribution of Sb is almost negligible. But it is interesting to note that the magnetic moment contributed by Sb-atom is negative, which indicates that the contribution from 5*p* states of Sb atom is anti-parallel to the magnetic moment contributed by Dy-4*f* states.

4. Conclusions

We have performed *ab initio* calculations of structural, magnetic, electronic and elastic properties of DySb in the B1 and high pressure B2 phases using LSDA + U method. It is found to be stable in ferromagnetic phase at ambient and high pressure conditions. Under compression it transforms from six fold coordinated B1 phase to eight fold coordinated B2 phase. We have investigated elastic properties at ambient and high pressures conditions. The material which is brittle at ambient conditions becomes ductile in B2 phase and its ductility increases under pressure. The LSDA + U method gives semi-metallic nature of DySb at ambient conditions with the proper splitting of *f*-bands in spin-up and down channels. We wish to point out that the Coulomb repulsion (U) strongly influences the elec-

tronic structure of DySb particularly in the treatment of correlation effects. The calculated local and total magnetic moment decreases with increasing pressure. Our calculated results on DySb are generally in good agreement with the available experimental data. Such types of effort are very scantly dedicated for RE monopnictides and hence require more experimental attention.

Acknowledgments

This work has been supported by the Department of Science and Technology (DST), New Delhi. SK is particularly thankful to CSIR, New Delhi for the award of Senior Research Fellowship. Thanks are due to Prof.(s) S. Auluck and R. Prasad for valuable discussion and suggestions during this work. We are also thankful to Prof. P. Blaha for providing WIEN2k code.

References

[1] I. Shirotani, J. Hayashi, K. Yamanashi, N. Ishimatsu, O. Shimomura, T. Kikegawa, Phys. Rev. B 64 (2001) 132101.
[2] M.E. Mullen, B. Lüthi, P.S. Wang, E. Bucher, L.D. Longinotti, J.P. Maita, H.R. Ott, Phys. Rev. B 10 (1974) 186.
[3] F. Hullinger, in: K.A. Gchneidnet, L. Eyring (Eds.), Hand Book of Physics and Chemistry of Rare Earths, vol. 4, Amsterdam, North Holland, 1979, p. 153.
[4] U. Bendict, W.B. Holzapfel, in: K.A. Gschneidnet, L. Eyring, G.H. Lander, G.R. Choppin (Eds.), Hand Book of Physics and Chemistry of Rare Earths, North Holland, Amsterdam, 1993, Chapter 17, p. 245.
[5] H. Takahasi, T. Kasuya, J. Phys. C 18 (1985) 2695.
[6] M. De, S.K. De, J. Phys. Chem. Sol. 60 (1999) 337.
[7] C.G. Duan, R.F. Sabirianov, W.N. Mei, P.A. Dowben, S.S. Jaswal, E.Y. Tsymbal, J. Phys.: Condens. Matter 19 (2007) 315220.
[8] D.C. Gupta, S. Kulshrestha, J. Phys. Soc. Japan 79 (2010) 044605.
[9] G. Pagare, D. Sen, V. Srivastava, S.P. Sanyal, J. Phys. Conf. Ser. 215 (2010) 012114.
[10] A. Bouhemadou, R. Khenata, M. Maamache, J. Mol. Struct.: THEOCHEM 777 (2006) 5.
[11] A. Bouhemadou, R. Khenata, M. Sahnoun, H. Baltache, M. Kharoubi, Physica B 363 (2005) 255.
[12] S. Lebègue, A. Svane, M.I. Katsnelson, A.I. Lichtenstein, O. Eriksson, J. Phys.: Condens. Matter 18 (2006) 6329.
[13] M. Horne, P. Strange, W.M. Temmerman, Z. Szotek, A. Svane, H. Winter, J. Phys.: Condens. Matter 16 (2004) 5061.
[14] H. Taub, C.B.R. Parente, Solid State Commun. 16 (1975) 857.
[15] J.S. Kouvel, T.O. Brun, F.W. Korty, Physics B + C 86–88 (1977) 1043.
[16] W.J. Hu, J. Du, B. Li, Q. Zhang, Z.D. Zhang, Appl. Phys. Lett. 92 (2008) 192505.
[17] P.W. Anderson, Rev. Mod. Phys. 50 (1978) 191.
[18] V.I. Anisimov, I.V. Solovyev, M.A. Korotin, M.T. Czyzyk, G.A. Sawatzky, Phys. Rev. B 48 (1993) 16929;
A.I. Liechtenstein, V.I. Anisimov, J. Zaanen, Phys. Rev. B 52 (1995) R5467.
[19] E. Sjöstedt, L. Nordström, D.J. Singh, Solid State Commun. 114 (2000) 15.
[20] P. Blaha, K. Schwarz, G.K.H. Madsen, D. Kvasnicka, J. Luitz, WIEN2k, An Augmented Plane Wave+Local Orbitals Program for Calculating Crystal Properties, Karlheinz Schwarz, Techn. Universitat Wien, Austria, 2001, ISBN 3-9501031r-r1-2.
[21] P. Hohenberg, W. Kohn, Phys. Rev. 136 (1964) 864.
[22] W. Kohn, L.J. Sham, Phys. Rev. 140 (1965) 1133.
[23] G.K.H. Madsen, P. Novak, Eur. Phys. Lett. 69 (2005) 777.
[24] F.D. Murnaghan, Proc. Natl. Acad. Sci. U.S.A. 30 (1944) 244.
[25] D.C. Wallace, Thermodynamics of Crystals, John Wiley Sons, New York, 1972 (Chapter 1).
[26] I.N. Frantsevich, F.F. Voronov, S.A. Bokuta, in: I.N. Frantsevich (Ed.), Elastic Constants and Elastic Moduli of Metals and Insulators Handbook, Naukova Dumka, Kiev, 1983, pp. 60–180.
[27] D. Pettifor, Mater. Sci. Technol. 8 (1992) 345.
[28] Z. Sun, S. Li, R. Ahuja, J.M. Schneide, Solid State Commun. 129 (2004) 589.
[29] P. Wachter, M. Filzmoser, J. Rebizant, Physica B 293 (2001) 199.
[30] H. Yamada, T. Fukawa, T. Muro, Y. Tanaka, S. Imada, S. Suga, D.X. Li, T. Suzuki, J. Phys. Soc. Japan 65 (1996) 1000.
[31] F. Leuenberger, A. Parge, W. Felsch, K. Fauth, M. Hessler, Phys. Rev. B 72 (2005) 014427.